Biosensors and Bioelectronics 142 (2019) 111493

Contents lists available at ScienceDirect

Biosensors and Bioelectronics

journal homepage: www.elsevier.com/locate/bios

Flexible, multichannel cuff electrode for selective electrical stimulation of the mouse trigeminal nerve

Jihye Bong[a,1], Jared P. Ness[b,1], Weifeng Zeng[c], Hyungsoo Kim[a], Joseph Novello[b], Jane Pisaniello[b], Wendell B. Lake[d], Kip A. Ludwig[b,d], Justin C. Williams[b,d], Zhenqiang Ma[a], Aaron J. Suminski[b,d,*]

[a] Department of Electrical and Computer Engineering, University of Wisconsin-Madison, Madison, WI, USA
[b] Department of Biomedical Engineering, University of Wisconsin-Madison, Madison, WI, USA
[c] Department of Surgery, School of Medicine and Public Health, University of Wisconsin-Madison, Madison, WI, USA
[d] Department of Neurological Surgery, School of Medicine and Public Health, University of Wisconsin-Madison, Madison, WI, USA

ARTICLE INFO

Keywords:
Flexible electronics
Selective stimulation
Bipolar cuff electrode
Trigeminal nerve stimulation
Somatosensory evoked potential

ABSTRACT

The trigeminal nerve (cranial nerve V), along with other cranial nerves, has in recent years become a popular target for bioelectric medicine due to its direct access to neuromodulatory centers. Trigeminal nerve stimulation is currently being evaluated as an adjunctive treatment for various neurodegenerative and neuropsychiatric diseases despite the mechanism of action being in question. In this work, we describe the development and validation of a novel neural interface for the infraorbital branch of the trigeminal nerve utilizing a thin film (TF) nerve cuff containing multiple electrode sites allowing for more selective stimulation of the nerve. We characterized the properties of the device using electrochemical impedance spectroscopy, cyclic voltammetry, voltage excursions, and *in vivo* testing. Electrochemical measurements demonstrate that the platinum-based electrodes possess a capacitive charge carrying mechanism suitable for stimulation of biological tissue with a safe charge injection limit of 73.13 μC/cm^2. *In vivo* stimulation experiments show that the TF cuff can reliably stimulate nerve targets eliciting cortical responses similar to a silicone cuff electrode. Furthermore, selecting different pairs of stimulation electrodes on the TF cuff modulated the magnitude and/or spatial pattern of cortical responses suggesting that the device may be able to selectively stimulate different parts of the nerve. These results suggest that the TF cuff is a viable neural interface for stimulation of the infraorbital branch of the trigeminal nerve that enables future research examining the therapeutic mechanisms of trigeminal nerve stimulation.

1. Introduction

Over the past two decades, cranial nerves have become attractive targets for novel neuromodulation therapies aimed at treating a variety of neurodegenerative disorders (Farrand et al., 2017), neuropsychiatric disorders (Cook et al., 2013; DeGiorgio et al., 2011; Milby et al., 2008), epilepsy (DeGiorgio et al., 2011; Fanselow et al., 2000; Milby et al., 2008; Pop et al., 2011), pain (Young, 1995), and promoting recovery following acute injury to the nervous system (Chiluwal et al., 2017; Ganzer et al., 2018). Vagus nerve stimulation (VNS) has received the most attention and is currently indicated as an adjunctive therapy for epilepsy and major depressive disorder (see Beekwilder and Beems, 2010 for a review). Recently, electrical stimulation of various branches of the trigeminal nerve (cranial nerve V) has emerged as an alternative to VNS due to its superficial course, potentially improved side effect profile and projections to similar cortical and subcortical targets (Fisher, 2011; Henry et al., 1998). Like VNS, trigeminal nerve stimulation (TNS) is known to result a reduction of seizure activity and improvement in measures of depression severity in both preclinical animal models and human trials (Cook et al., 2013; DeGiorgio et al., 2011, 2009; Fanselow et al., 2000; Pop et al., 2011) and has recently received FDA approval to treat ADHD in 7–12 year old children. Despite these promising data, there remains a lack of knowledge about the mechanism of action by which TNS modulates the central and peripheral nervous system to therapeutic effect (Fanselow et al., 2000).

While preclinical studies examining efficacy and translational

* Corresponding authorDepartment of Neurological Surgery University of Wisconsin-Madison, 600 Highland Ave, Madison, WI, 53792, USA.
E-mail address: asuminski@wisc.edu (A.J. Suminski).
[1] Denotes Equal Contribution.

https://doi.org/10.1016/j.bios.2019.111493
Received 1 February 2019; Received in revised form 26 June 2019; Accepted 3 July 2019
Available online 05 July 2019
0956-5663/

potential of new medical technology are well suited for rat and large animal models, initial mechanistic studies are often conducted in mouse models due to the available genetic tools and techniques for dissecting neural circuits and physiological function. The use of mouse models to examine the therapeutic mechanisms of TNS has been limited by available instrumentation to reliably deliver local electrical stimulation to cranial nerve targets. Many traditional methods for interfacing with peripheral nerves (i.e. extraneural cuff and intrafasicular electrodes; (Boretius et al., 2010; Tyler and Durand, 2002; Veraart et al., 1993; Yoshida and Stein, 1999); see Micera and Navarro, 2009 for a review) are not well suited for mouse models of TNS due to the constraints imposed by mouse anatomy (nerve size and available space) and the potential for trigeminal injury to cause severe chronic pain (Ma et al., 2012). Instead, some have employed a variety of microfabrication techniques, including photolithography (Caravaca et al., 2017; Plachta et al., 2014) and nanoscale 3d printing (Lissandrello et al., 2017), to create low profile devices for neuromodulation of small cranial nerves using electrical stimulation. Unfortunately, some of these devices do not currently provide the ability to selectively activate different functional components within the nerve like those interfaces designed for larger peripheral nerves (Tyler and Durand, 2002, 1997; Veraart et al., 1993) because they lack multiple stimulation sites (a notable exception being the VNS electrode presented by Plachta et al.). Thus, there is a need for multi-channel electrode technology that is well optimized to selectively stimulate small cranial nerves to enable future mechanistic research on TNS.

Here we describe the development and validation of a flexible, 10-channel thin film (TF) nerve cuff electrode that enables future mechanistic research on TNS. The goals of this effort are threefold: 1) to create a neural interface well fit to the unique anatomy of the infraorbital branch of the mouse trigeminal nerve, 2) to demonstrate that the electrochemical properties of the interface are well suited for electrical stimulation of the nerve and 3) to show that the multichannel electrode design is capable of selective stimulation of the nerve. The electrochemical properties of the TF nerve cuff electrodes, measured using electrical impedance spectroscopy (EIS), equivalent circuit modeling, cyclic voltammetry (CV), and voltage excursions, are consistent with previously reports on platinum electrodes and demonstrate the ability of the device to safely stimulate the infraorbital branch of the trigeminal nerve. The ability of the TF cuff electrode to selectively stimulate the infraorbital nerve is examined by measuring local field potential (LFP) responses over the somatosensory cortex evoked by stimulation of different cathode/anode pairs on the device. Both the amplitude and spatial pattern of cortical responses are modulated by the selection of stimulation channel pairs causing stimulation through the TF cuff to better resemble naturalistic stimulation (air puff to whiskers) compared to a traditional bipolar cuff electrode. This work demonstrates that the TF cuff electrode is a viable interface for reliably activating the trigeminal nerve and may be a useful tool to examine the therapeutic mechanisms of TNS and other neuromodulation therapies.

2. Materials and methods

2.1. Device Fabrication

2.1.1. Thin film (TF) nerve cuff

The TF nerve cuff device was fabricated on an insulative, flexible and biocompatible substrate polymer, Parylene C, using previously described techniques (Richner et al., 2014). Briefly, a silicon wafer was first coated with 10 μm of Parylene C using the chemical vapor deposition (CVD) process (Fig. 1a). Next, a thin metal layer (10 nm Ti/230 nm Au/10 nm Pt) was deposited to form electrodes and connection pads followed by a second 10 μm layer of Parylene C. A photolithography and a reactive ion etch (RIE) were used to open the substrate for suture holes and expose the metal electrodes prior to the devices being released from the silicon wafer. Our current TF cuff design draws inspiration from two other recently published multi-contact, thin film electrodes targeted for VNS in rodent models (Caravaca et al., 2017; Plachta et al., 2014) Like Caravaca et al. and Plachta et al., we chose a modular design with multiple electrode layout geometries to increase the flexibility of the overall design. Our TF nerve cuff design features a total of 10 bar-shaped electrodes, measuring 50 μm × 500 μm, arranged as two groups of five electrodes mirrored on the face of the device (Fig. 1b). Each group consists of a bipolar (electrodes 1:9 and 2:10; 1750 μm spacing) and a tripolar (electrodes 3:5:7 and 4:6:8; 275 μm spacing) set of electrodes to offer a multitude of possible configurations for electrically stimulating the nerve or recording evoked potentials. In addition, the device contains four holes located at each corner to aid in wrapping/securing the device around the nerve with suture (Fig. 1a–b).

2.1.2. Silicone (Si) nerve cuff

In addition to the TF nerve cuff, we fabricated a bipolar cuff electrode allowing us to compare the ability of each device to activate the infraorbital nerve. We used fabrication methods described previously for vagus nerve cuffs with modifications in size to accommodate the anatomy of the mouse (Childs et al., 2015). Briefly, these custom bipolar cuff electrodes were fabricated by inserting 2 platinum-iridium wires (50.8 μm bare diameter, AM Systems, Part #: 776000) through a silicone tube (3 mm length, 635 μm inner diameter, AM Systems Part #: 806700) with 1 mm inter-electrode spacing. The insulation around the wire inside the cuff was removed and the wires were anchored to the tube using a silicone adhesive (KwikSil, World Precision Instruments). Each wire was terminated with a pin receptacle (Mil-Max Manufactruing, Part # 9407-0-15-15-11-27-10-0) to facilitate connection to the stimulator.

2.2. Electrochemical measurement

To characterize the electrochemical properties of the TF nerve cuff, we performed electrochemical impedance spectroscopy and cyclic voltammetry using an Autolab PGSTAT 128N (Metrohm Autolab, Netherlands). A three-electrode system was employed where: one of the TF nerve cuff electrodes served as the working electrode (WE), a large platinum sheet served as the counter electrode (CE), and a non-current carrying Ag/AgCl electrode served as the reference. The EIS and CV tests were performed with each electrode submerged in saline solution (0.9% w/v sodium chloride) and in the atmosphere. EIS was performed using 10 mV sine waves at frequencies from 0.1 to 100 kHz, and the parameters of the equivalent circuit were extracted using Nova 1.10 (Metrohm Autolab, Netherlands). For CV, three cycles of a potential sweep from −0.6 V to 0.8 V with a step potential of 2.44 mV were applied, but only the stabilized signal curve of last cycle was plotted. Cyclic voltammetry at scan rates of 10–1000 mV/s was performed. In addition, we measured the charge injection capacity (CIC) of the TF nerve cuff electrode using the voltage excursion method (Cogan, 2008; Wilks et al., 2017). A total of ten charge-balanced, constant-current pulses (25–200 μA, cathode leading, 500 μs phases, 100 μs gap between phases) were applied to the WE (return path through the CE) using a TDT IZ2H stimulator (Tucker-Davis Technologies, Alachua, FL), and the resulting voltage excursion was measured between the WE and RE using a Digilent Analog Discovery Oscilloscope (Digilent Inc., Pullman, WA). We computed the average of the final 8 voltage excursion time series and measured the maximum negative polarization potential, E_{mc} (i.e. the measured voltage on the WE 50 μs following the end of the cathodic phase).

2.3. Animal surgery

Three C57BL/6 mice (2 female) between the ages of 8 and 32 weeks were used during the course of this study to examine the viability of the thin-film neural interface. All animal procedures were reviewed and

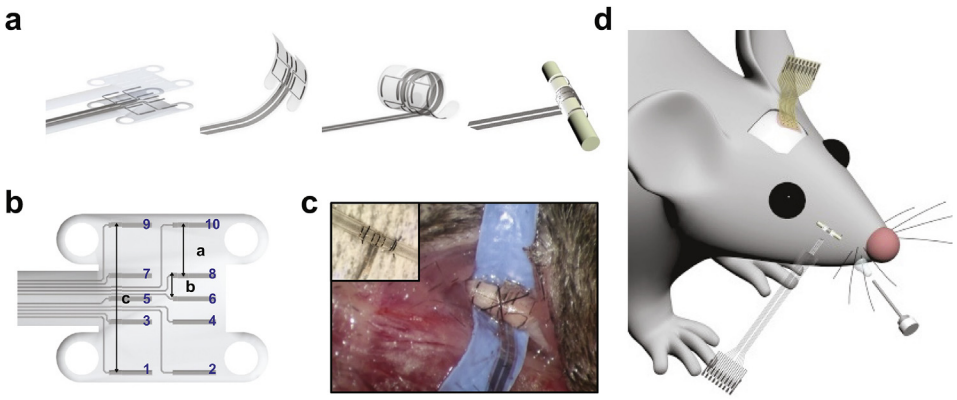

Fig. 1. Fabrication, features and implantation methodology for the TF nerve cuff. (a) The flexibility of the TF cuff allows it to be easily wrapped and conform to the circumference of a nerve. (b) Electrode spacing with electrode sites numbered for reference, a: 600 µm, b: 275 µm, and c: 1750 µm. Electrode site size is 50 µm × 500 µm. Suture holes on the four corners of the array anchor the cuff wrapped up to the nerve. (c) An example of the TF cuff implanted on a mouse infraorbital nerve. Inset (above) shows the TF cuff wrapped around a Silicone tube. (d) Cartoon depicting the experimental paradigm showing both electrical and naturalistic, air puff of the whisker pad, stimulation of the infraorbital nerve. Responses are recorded contrallaterally through a epidurally implanted µECoG.

approved by the Institutional Animal Care and Use Committee (IACUC) at the University of Wisconsin-Madison. Mice were housed on a 12-h light/dark cycle with ad libitum access to food and water. Prior to the terminal surgical procedure, we administered a bolus injection of 0.25 ml 0.09% saline to maintain fluid volume and dexamathasone (2 mg/kg, AgriLabs) to reduce the potential of cerebral edema due to the surgical manipulations. Following induction (5% isoflurane gas in 100% O_2), mice were placed into a stereotaxic head holder, the scalp and snout were shaved (sparing the mystacial pad and whiskers), and the skin was prepped with alternating povidone iodine and alcohol scrubs. Anesthesia was maintained at (1.0–2.5% isoflurane gas in 100% O_2) throughout the duration of the surgical procedures. Heart rate, blood oxygen saturation and body temperature were monitored throughout and a water-circulated heating blanked helped to regulate body temperature (PhysioSuite, Kent Scientific).

We chose an anterio-medial surgical approach to access the infraorbital nerve (see Dingle et al., 2019 for details). Regardless of the type of cuff that was implanted, a 1 cm incision was made along the midline between the eyes and nose stopping before the soft tissue of the nose. Skin was retracted revealing the underlying muscle, which was bluntly dissected away from the nasal bone revealing the infraorbital nerve exiting the infraorbital foramen. The nerve was carefully dissected from surrounding soft tissue and a piece of sterile glove was placed under the nerve. Next, either the Si or TF cuff electrode (see Device Fabrication) was placed under the nerve and the nerve gently lowered into the electrode.

To verify engagement between the nerve and cuff electrode, we implanted a custom 16-channel micro-electrocorticography (µECoG) array on top of the dura over the barrel field of the somatosensory cortex contralateral to the cuff implant (Richner et al., 2014). Here, the scalp was incised exposing the skull, which was then cleaned and dried. A ~4 mm × 4 mm section of skull, centered −1 AP and −4 ML from bregma, was removed using a surgical drill. The electrode array was then placed on the dura with a micromanipulator and its edges were covered with saline soaked gelfoam. The array's platinum ground and reference wires were coiled around a screw that was placed head side down on the skull above the contralateral hemisphere.

2.4. Electrophysiology

To investigate the viability of the TF cuff electrode as a neural interface, we used the µECoG array to measure cortical LFPs evoked by direct electrical stimulation of the nerve. For comparison, we recorded LFP evoked by stimulation of the nerve using the Si cuff electrode and by direct stimulation of the whiskers/whisker pad using an air puff (10 m s duration). Cortical responses evoked by stimulation were amplified (2×), bandpass filtered (corner frequencies: 2.2 Hz–2.7 kHz) and then digitized at 6 kHz using a PZ5 NeuroDigitizer and a RZ5d BioAmp Processor (Tucker-Davis Technologies, Alachua, FL). Here, electrical stimuli consisted of single, charge-balanced, cathode leading, biphasic pulses (200 µs phase duration) with amplitudes ranging from 50 µA to 500 µA. Stimuli were generated using an IZ2H stimulator (Tucker-Davis Technologies, Alachua, FL). Stimulation pulses for a single current amplitude were applied at pseudorandom intervals (3–4 s spacing) over an approximately 1 min stimulation trial (16–19 stimulation instances per current amplitude). The cathode of the bipolar stimulating electrodes was always defined as the most rostral electrode (i.e. closest to the brain). Throughout this report, we denote the stimulation electrodes on the TF nerve cuff with the cathode listed first (i.e. 2:10 where electrode 2 is the cathode and electrode 10 is the anode). Importantly, anesthesia was switched from isoflurane to a ketamine (25–100 mg/kg) and dexmedetomidine (0.05–0.1 mg) cocktail 20 min prior to the start of recording as isoflurane is known to reduce cortical activity.

2.5. Data analysis

Our interest was to examine how evoked responses in the somatosensory cortex varied based on the type of stimulation (electrical or naturalistic) and cuff. To this end, we bandlimited LFP measured with the (µECoG) array using a 2nd order, Butterworth lowpass filter (cutoff frequency = 500 Hz), removed line noise using a 3rd order notch filter (cutoff frequencies = 55 Hz and 65 Hz) and computed the average of evoked responses from the same stimulus amplitude and channel. We quantified changes in the magnitude of the somatosensory evoked potentials (SSEPs) by measuring the peak to peak amplitude of the evoked response for each pair of stimulation electrodes on the TF nerve cuff. The positive and negative going peaks were defined as the average of 7 data points centered at the maximum and minimum points of the response (not including the stimulation artifact). Baseline activity was defined as the average LFP measured during a 20 m s time period prior to the onset of the stimulation. One-way ANOVA and post hoc Tukey-Kramer t-tests were used to examine the effect of current amplitude on the magnitude of the SSEP. We were also interested in quantifying the ability of the TF cuff electrode to modulate cortical responses based on selection of stimulating electrodes. Here, heatmaps describing the spatial organization of cortical activity evoked through TF cuff stimulation were obtained by normalizing peak to peak SSEPs by the maximum peak to peak SSEP measured on any µECoG electrode across all stimulating electrode pairs. Normalized responses were interpolated using a cubic interpolation algorithm (Matlab function griddata) to a meshgrid with 1 µm resolution (for visualization purposes). Two-way ANOVA with post hoc Tukey Kramer t-tests were used to investigate the effect of the choice of stimulation electrode pairs on the peak to peak SSEP magnitude. The recording electrode on the µECoG array was considered a random factor in these tests. Finally, a cross correlation

analysis was used to examine differences in spatial organization of neural activity elicited by stimulation on different electrode pairs on the TF nerve cuff electrode. We computed the correlation coefficient (Matlab function corrcoef) between arrays of peak to peak SSEP amplitudes containing all active channels on the μECoG array for each of the different stimulation electrode pairs. We used the 95% CI about zero correlation (i.e. $95\%\ CI \cong 2\sqrt{\#\ channels}$; Box et al., 2015) to assess changes in the responses elicited by stimulation on different electrode pairs.

3. Results and discussion

3.1. Electrochemical characterization

The functional electrode for the TF Cuff exposed to the electrolyte/tissue was a 10 nm thick layer of platinum, with an underlying 230 nm thick layer of gold. Platinum and gold are both established biocompatible electrode materials that are well described for stimulating and recording in chronic in-vivo animal experiments and for human diagnostic and therapeutic applications (Brummer and Turner, 1977; Ludwig et al., 2011; Penry and Dean, 1990; Walton et al., 1987; Wei and Grill, 2009). To assess the electrochemical behavior of the resulting electrode/electrolyte interface after fabrication, three analysis techniques were performed: Cyclic Voltammetry, Electrochemical Impedance Spectroscopy, and Voltage Excursions. Not only are these techniques common for characterize the electrode/electrolyte interface in academic studies (Merrill et al., 2005), they are often used as part of the core foundation to support safety for chronic stimulation for regulatory approval by the Food and Drug Administration (Wilks et al., 2017).

Cyclic voltammetry is traditionally performed to identify stereotypical electrochemical reactions for the electrode material directly in contact with the electrolyte, as well as identify any unanticipated electrochemical reactions that occur at the electrode/electrolyte interface that may indicate issues/impurities arising from the manufacturing process (Cogan, 2008; Merrill et al., 2005). For evaluating platinum and gold electrodes with cyclic voltammetry (CV), the applied potential is swept between −0.6 and 0.8 V versus an Ag/AgCl reference, which represent the boundaries at which hydrogen and oxygen evolution begin to occur, respectively (Cogan, 2008; Trevathan et al., 2019). As these reactions result from the electrolysis of H_2O in the electrolyte solution, these boundaries are commonly referred to as the 'water window'. These reactions are assumed damaging to tissue as they alter local pH and can generate platinum/gold salts which can be toxic depending on concentration. Consequently, the overall charge that can be delivered at potentials within the 'water window' – known as the charge storage capacity (CSC_c) of the electrode - is a common measure of charge that can be delivered safely without tissue damage.

Cyclic voltammetry swept within the known water window for Pt/Au was used to examine the presence of electrochemical reactions and calculate cathodal charge storage capacity (CSC_c) on the surface of Pt electrodes (Fig. 2a). The CV response is known to vary as the sweep rate is increased from 10 to 1000 mV/s, although the faradaic electrochemical reactions remain unchanged, the increase in sweep rate changes non-faradaic capacitive charging of the electrode (Cogan, 2008). As expected, clear current peaks in the CVs are evident at ~-0.6 V and 0.8 V respectively representing the start of hydrogen and oxygen evolution respectively (Fig. 2a). Similarly, peaks are also evident at ~0 V and −0.2 V, which shift slightly depending on the sweep rate. These peaks are stereotypical for platinum electrodes, and represent the reversible oxidation and reduction of the chloride ion with the platinum surface (Hudak et al., 2010; Kumsa et al., 2016). Hydrogen plating reactions which are common for platinum electrodes immediately before the cathodic potential for hydrogen evolution were not observed. This result is not unexpected, as harsh sonication/cleaning steps are often needed to remove platinum oxides that naturally occur at the exposed surface in air over time to observe hydrogen plating reactions; these steps were deliberately not performed as they are not necessary to ensure electrode safety and could leave residuals on the surface that is problematic to tissue in-vivo if not completely removed.

CSC_c, was calculated from the time integral of the cathodic current in a cyclic voltammogram over the applied potential range (Cogan, 2008). The shaded region in the Parylene-insulated Pt electrode's CV in Fig. 2a represents a CSC_c of 0.155 mC/cm^2, calculated at a sweep rate of 20 mV/s. This is within the range of CSC_c reported for Pt electrodes of 0.55 mC/cm^2 at 20 mV/s in phosphate buffered saline (Cogan, 2008), with any difference likely being attributable to small differences in pretreatment/cleaning before measurements.

Although CVs provide a detailed assessment of electrochemical behavior at the electrode/electrolyte interface, the triangle CV waveform applied is much longer and is fundamentally different in shape compared to the biphasic square wave pulses typically used to activate nervous tissue safely in-vivo. Consequently, the calculated CSC_c from a CV is known to dramatically overestimate the charge density that can be safely applied before deleterious tissue reactions occur (Cogan, 2008; Wilks et al., 2017). To assess the safety using the actual stimulation pulses of interest for activating tissue, voltage excursions are preferred. During voltage excursions, applied charge density given cathodic-leading, biphasic, square wave pulses commonly used for the activation of tissue. The amplitude of these pulses is gradually increased until −0.6 V of polarization on the electrode (E_{mc}) is measured, which represents the charge density limit that can be safely applied before unwanted hydrogen evolution occurs. This limit is known as the as charge injection capacity (CIC) (Cogan, 2008).

E_{mc} is computed from the difference of the resting equilibrium potential (E_e) to the residual voltage (R_v) left on the electrode just after the stimulus (Fig. 2b). Stimuli ranging from 50 μC/cm^2 to 200 μC/cm^2 were passed through a single electrode site of the TF cuff. At 50 μC/cm^2 we report a E_{mc} of −0.39 V well within the safe parameters of CIC. As we increased our current stimulus greater and greater E_{mc} values were measured, ultimately crossing the safe limits threshold of −0.6 V (Fig. 2c). In order to extract CIC from this data, we fit a least-squares 3rd order polynomial curve ($R^2 = 0.9942$) to these data points, resulting in 73.13 μC/cm^2 as our safe charge limit. These calculated limits are consistent with the range of 50–150 μC/cm^2 expected for platinum electrodes from multiple reviews (Cogan, 2008; Cogan et al., 2016). Limits given at or below this value will overtime will not cause hydrolysis leading to damaged tissue or breakdown of the TF electrode.

Unlike CVs and Voltage Excursions which are intended to assess the electrochemical behavior at the electrode/electrolyte interface at the large charge densities needed for the activation of nervous tissue, Electrochemical Impedance Spectroscopy (EIS) is used to assess behavior of the electrode/electrolyte interface during the application of very low voltage sinusoidal pulses mimicking the extracellular potential generated by neural activity. As a shorthand, the impedance measured is often reported only at 1 kHz, as the power calculated from a recorded action potential generated by a nerve is greatest at 1 kHz (Kuffler and Nicholls, 1976; Ludwig et al., 2006; Williams et al., 2007). Higher electrode impedances can increase thermal noise to the point where it dominates all other sources of noise, and increase loss of current from the Ti trace connecting the electrode to the recording instrumentation through the insulating layer, known as 'shunt loss' (Ludwig et al., 2006). Impedances at 1 kHz of 10 MΩ or greater can reduce signal to noise to an extent that recording neural activity extracellularly becomes problematic (Ludwig et al., 2011). The average impedance of the 10-channel was 11.06 kΩ with standard deviation of ± 1.63 kΩ for electrodes with an area of 25,000 μm^2 (n = 50, 10 sites per each 5 devices). This is well within the 1 kHz impedance range for epineural recording cuffs reported in other studies (Akin et al., 1994).

The Bode modulus and phase plot depict expected impedance and phase characteristics expected for platinum/gold recording electrodes over the 0.1 Hz to 100 kHz frequency range (Fig. 2d–e). The most

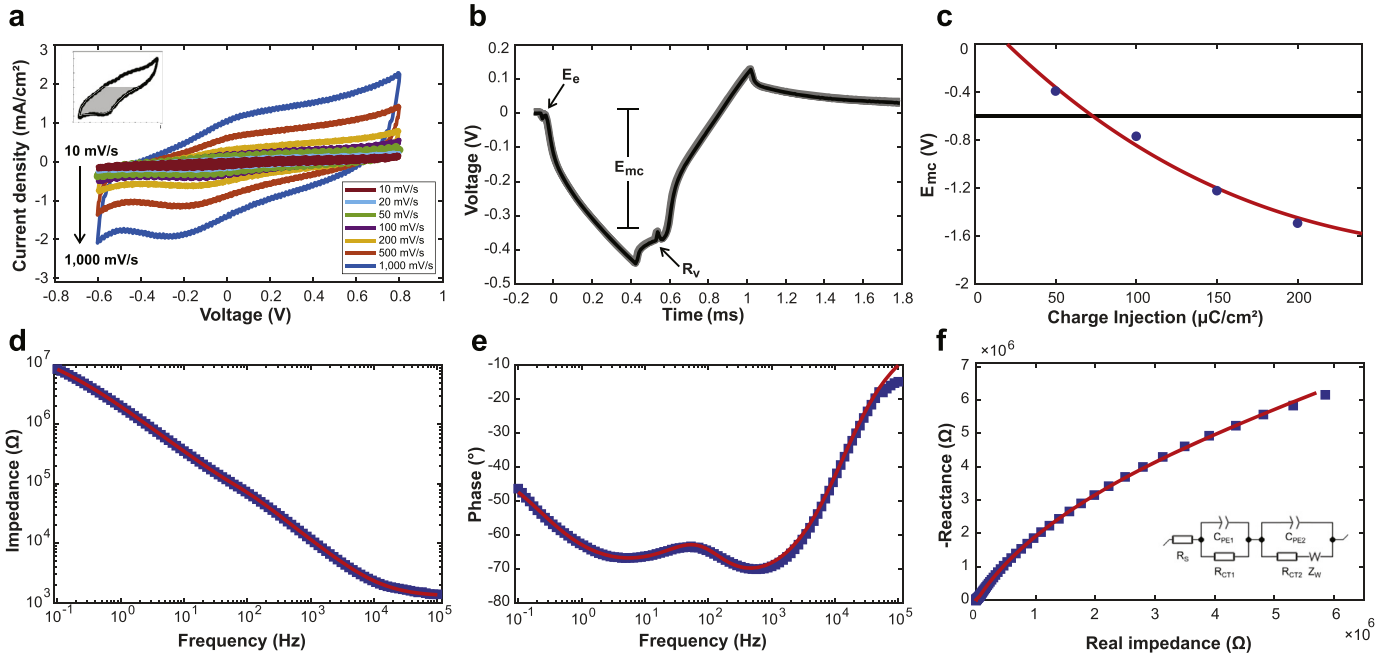

Fig. 2. (a) CV for varying scan rates and representative CV from the channels (inset). (b) Average voltage excursion at 50 μC/cm^2 through a single TF nerve cuff electrode site. The pulse given was charge balanced and biphasic with a 500 μs pulse duration and an interpulse period of 100 μs. The maximum negative polarization potential (E_{mc}) was obtained from the difference of the residual voltage (R_v) and the equilibrium voltage (E_e) giving in this case $E_{mc} = -0.39$ V. (c) A least-squares polynomial fit of E_{mc} values gathered from increasing stimulation shown in charge density. A threshold at -0.6 V denotes the CIC limit of the TF cuff at 73.13 μC/cm^2. (d) Bode magnitude plot and (e) Bode phase plot with measurement data and equivalent circuit modeling of a TF nerve cuff. (f) Nyquist plot of measurement data and modeling of a TF nerve cuff electrode with the equivalent circuit (inset).

common circuit representation of a platinum or gold electrode is the Randles circuit, which in its most simple form consists of a solution resistance, R_s, in series with a capacitor and resistor in parallel, C_{DL} and R_{CT} respectively. C_{DL} represents the capacitance of the electrode/Helmholtz double layer, whereas R_{CT} represents the impedance of electrochemical reactions at the electrode/electrolyte interface. At very high frequencies like 100 kHz, the impedance of C_{DL} is very low compared to the solution resistance R_s as the impedance of a capacitor is inversely proportional to the frequency applied. Hence the impedance of the overall system is dominated by R_s, as indicated by the phase angle at 100 kHz approaching zero. As the frequency decreases from 100 kHz to approximately 1 kHz the impedance of C_{DL} increases and begins to dominate the impedance of the overall circuit, as indicated by the phase angle approaching $-90°$. At frequencies lower than 1 kHz, the impedance of the capacitive pathway C_{DL} increases even more, and significant current begins to flow through electrochemical reactions at the platinum electrode/electrolyte interface represented by the parallel element R_{CT}. The general form of the impedance and phase plots for the Pt TF Cuff electrodes is fairly well described by this simple circuit.

To improve the fit of the circuit model to realistic electrode/electrolyte behavior, it is common to replace C_{DL} with a constant phase element (C_{PE}), which better describes the non-ideal capacitive behavior of the electrode/electrolyte double-layer interface. In addition a Warburg element, Z_w, is often placed in series with R_{CT} to better represent the diffusion of ions to the electrode surface as electrochemical reactions occur. We observed that the inclusion of a C_{PE} and Z_w improved the reconstruction of the TF Cuff electrode behavior in the impedance, reactance, and phase plots it did not fully capture the small hump in phase starting at 10 Hz and ending at ~1 kHz (See Fig. 2d, e, and f). We found that this additional behavior could be better described by including in series an additional R_{CT2} and C_{PE2} in parallel to the normal Randles circuit, resulting in the circuit drawn in the inset of Fig. 2f. This strategy has previously been employed to account for the formation of oxides at the electrode surface, which would be expect of a platinum or gold electrode exposed to air (Hitz and Lasia, 2001).

Fitting the model described in Fig. 2f to the measured data yields an equivalent circuit with $R_s = 1.26$ kΩ, $R_{CT1} = 23.8$ kΩ, $R_{CT2} = 11.2$ MΩ. The C_{PE1}, C_{PE2} and Z_w parameters of the equivalent circuit model were estimated to be 0.67 nS s^1, 0.11 μS s$^{0.80}$, and 0.26 μS s$^{1/2}$ respectively. C_{PE} is defined as,

$$C_{PE}(w) = \frac{1}{Q(jw)^n}$$

where, j is the imaginary unit ($j^2 = -1$), ω is the angular frequency, and the CPS parameter Q represents the differential capacitance of the interface when $n = 1$. The predicted behavior of this model is very consistent of what would be expected from a primarily platinum electrode/electrolyte interface with oxides formed at the surface, and very well fits our measured data from the TF cuff electrodes. Combined with the CV and Voltage Excursion data, these data demonstrate that the resulting electrode electrochemical behavior is very consistent with well understood norms for platinum/gold electrodes, and is well within ranges necessary for safe activation of neural tissue or extracellular recording of neural activity.

3.2. In vivo experiments

To assess the feasibility and reliability of stimulation with the TF cuff, SSEPs were recorded in response to electrical stimulation of the infraorbital branch of the trigeminal nerve with either a Si or TF cuff electrode. The standard Si cuff (Fig. 3a inset) has two electrodes that wrap around the circumference of the nerve limiting the ability to target small structures within the nerve. On the other hand, the TF cuff (Fig. 3b inset) has an array of electrodes available, allowing different orientations of stimulation electrodes theoretically providing a more focal stimulus to the nerve.

Before evaluating the ability to the TF cuff electrode to selectively activate a nerve, we wished to verify that this new device performed similarly to a standard Si cuff electrode. Evoked SSEPs were measured in response to electrical stimuli applied through each cuff electrode

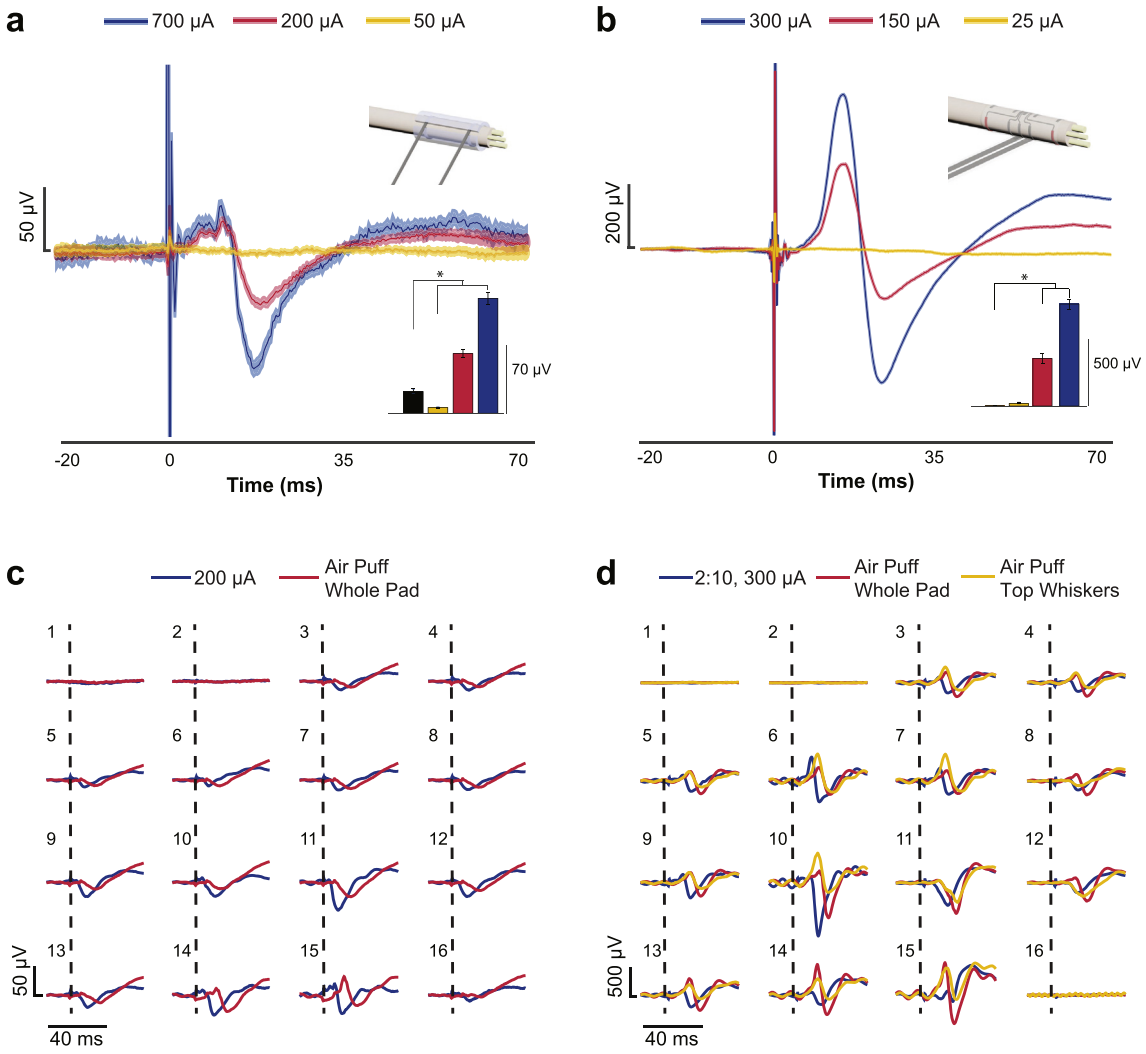

Fig. 3. Comparison cortical responses evoked by stimulation on the Si and TF nerve cuffs. (a and b) Exemplar single channelSSEPs recorded from the somatosensory cortex in response to stimulation on the two cuff electrodes. Note that the response magnitude increases as the magnitude of stimulation is increased. Insets (above) show a cartoon depiction of the corresponding stimulating cuff, for TF cuff stimulation electrodes highlighted in red. Insets (below) show average peak to peak SSEP amplitude measured in response to increases in stimulation current. Error bars represent ± 1 SE about the mean. Black brackets denote differences in SSEP amplitude resulting from stimulation on different electrodes at the $\alpha = 0.05$ level of significance. Black bar is average signal magnitude prior to the start of stimulation (See methods for details). (c and d) Cortical responses from all 16 channels of the µECoG array measured in response to both electrical (blue traces) and naturalistic (red and yellow traces) stimulation of the infraorbital branch of the trigeminal nerve. (For interpretation of the references to color in this figure legend, the reader is referred to the Web version of this article.)

where the electrode sites on the TF cuff were chosen to have similar orientation and spacing to the Si cuff (electrodes 2 and 10, see Fig. 1c). Responses evoked by stimulation had similar shape and onset latency ($22.2 \pm 2.4e^{-4}$ m s and $18 \pm 3.7e^{-4}$ m s for the TF and Si cuff stimulation, respectively), but the amplitude of the response was much larger when stimulation was applied through the TF cuff electrode (Fig. 3a–b). The latency of these responses are consistent with previous work examining the time delay between electrical stimulation of the infraorbital nerve and spiking activity in the somatosensory cortex (Fanselow and Nicolelis, 1999). The larger amplitude of cortical potentials evoked by TF cuff stimulation may be due to a variety of factors. First, the increased flexibility of the TF cuff compared to the Si cuff may provide better interface to the nerve (improving the contact between the stimulating electrodes and nerve) leading to better charge injection properties (Cogan, 2008). In addition, properties of the µECoG electrodes and their interface with the cortical surface could also contribute to these amplitude differences. Future work will investigate the source of these effects.

Regardless of the differences in amplitude of cortical responses evoked by stimulation with the two cuff electrodes, ANOVA found a significant effect of current amplitude on the magnitude of the SSEPs for both the TF and Si cuff electrodes ($F_{3,96} = 188.02$, $p = 4.7e^{-40}$; $F_{3,95} = 141.38$, $p = 6.56e^{-37}$). SSEPs measured in response to 200 and 700 µA stimuli applied with the Si cuff were significantly larger than baseline, as were evoked responses generated by stimulation at 150 and 300 µA on the TF cuff (Fig. 3a–b insets; $p < 0.05$; Tukey-Kramer post hoc t-test in both cases). To investigate whether the responses elicited using electrical stimulation were a reasonable proxy for naturalistic stimuli, we compared SSEPs evoked by a short air puff on the mystacial pad/whiskers to those evoked by electrical stimulation. When using the Si cuff electrode (Fig. 3c), we find that the spatial pattern of activity resembles stimulation of the entire mystacial pad, while stimulation through sites 2:10 on the TF cuff electrode generates a pattern of activity that resembles both stimulation of the mystacial pad and some individual whiskers (Fig. 3d).

Given the ability to elicit SSEPs using the TF cuff electrode, we wished to investigate how the choice of stimulation electrodes would impact the amplitude and spatial distribution of the evoked cortical

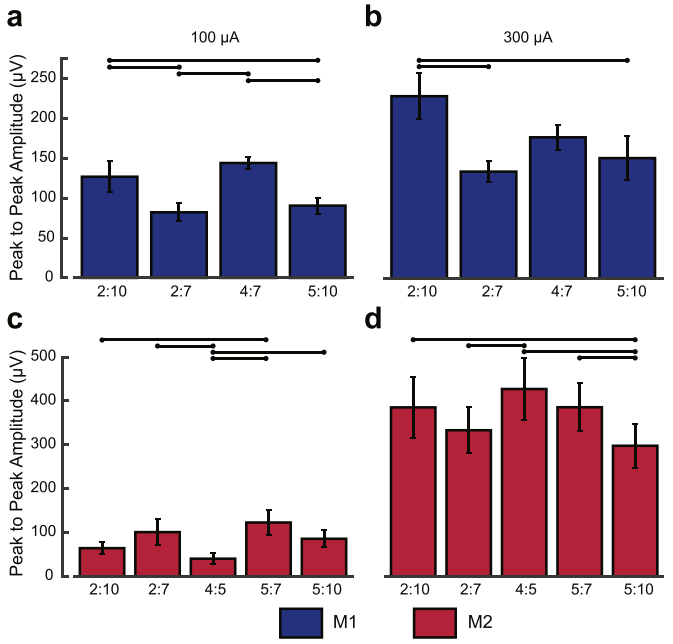

Fig. 4. Averaged peak to peak SSEP amplitude measured in response to stimulation on different TF cuff electrodes. The cathode is always listed first. Error bars represent ± 1 SE about the mean. Black brackets denote differences in SSEP amplitude resulting from stimulation on different electrodes at the $\alpha = 0.05$ level of significance. (a) SSEP amplitude for a 100 µA stimulation current in mouse M1. (b) SSEP amplitude for a 300 µA stimulation current in mouse M1. (c) SSEP amplitude for a 100 µA stimulation current in mouse M2. (d) SSEP amplitude for a 300 µA stimulation current in mouse M2.

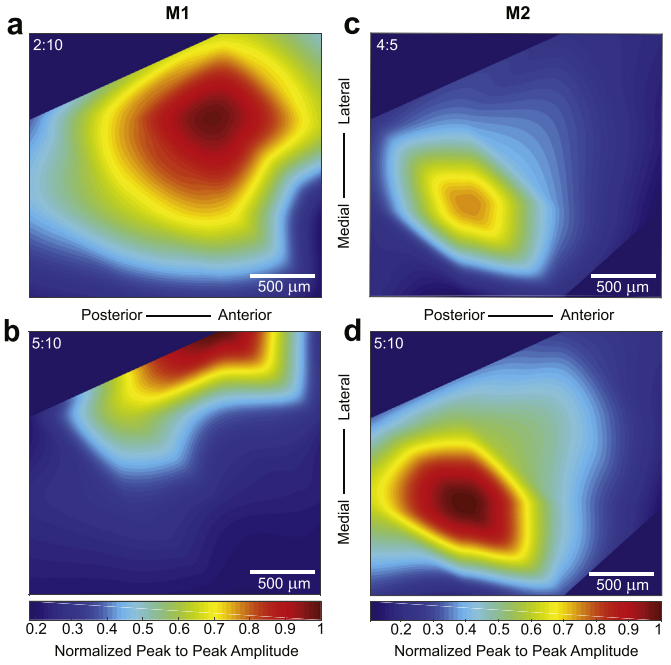

Fig. 5. Heatmap representation of cortical normalized peak to peak potentials in a given 16 channel µECoG array. (a and b) Spatial patterns of cortical activity evoked by 300 µA stimulation on electrodes 2:10 (a) and 5:10 (b) for mouse M1. Notice that the centroid of the cortical activity is different for the two stimulation conditions. (c and d) Spatial patterns of cortical activity evoked by 300 µA stimulation on electrodes 4:5 (a) and 5:10 (b) for mouse M1. Notice that the magnitude of the cortical activity is modulated by the choice of stimulation electrodes.

responses. Specifically, we compared cortical responses evoked by stimulation through 4 or 5 unique bipolar electrode pairs (M1 and M2, respectively) at two different current amplitudes (Fig. 4). In both mice we found that SSEP amplitude increased as the stimulation current was raised from 100 µA to 300 µA (paired t-test; $T_{55} = 7.85$, $p = 1.53e^{-10}$ and $T_{69} = 12.3$, $p = 4.73e^{-19}$ for M1 and M2, respectively). Furthermore, ANOVA found a significant effect of the selected pair of stimulation electrodes on the average peak to peak SSEP magnitude across the µECoG array for each mouse and stimulation amplitude (M1: $F_{3,39} = 17.81$, $p = 1.93e^{-7}$ and $F_{3,39} = 8.57$, $p = 2e^{-4}$; M2: $F_{4,48} = 11.77$, $p = 9.66e^{-7}$ and $F_{4,48} = 7.91$, $p = 5.58e^{-5}$ for 100 µA–300 µA currents, respectively). These results suggest that the selection of stimulation electrodes could be used to optimize the ability of the TF cuff electrode to elicit robust responses with minimal applied energy. Interestingly, we found that the pattern of average SSEP amplitudes from the different stimulation pairs varied for the different stimulation amplitudes (Fig. 4, significance bars) suggesting that different volumes of nerve may be influenced by the selection of stimulation electrodes.

Heatmaps of the normalized peak to peak SSEP amplitudes were used to visualize the spatial distribution of activation resulting from stimulation on different TF cuff electrode pairs. In comparing stimulation on the 2:10 pair to the 5:10 pair in M1, we find a medial shift in the activation focus on the cortical surface (Fig. 5a–b). The highly localized organization of the whisker system and its projection to the somatosensory cortex (Petersen, 2007) support the notion that this migration in the activation focus results from these configurations stimulating different fascicles within the infraorbital nerve. In contrast, comparing the 4:5 and 5:10 pairs in M2 do not result in a large shift in the activation focus (Fig. 5c–d), but rather show a strong potentiation in the magnitude of the response across the somatosensory cortex (i.e. lower amplitude SSEPs resulting from stimulation on the 4:5 pair). It is possible that reduced SSEP amplitude on the 4:5 stimulation pair may be attributed to the lack of separation between these stimulation electrodes as current density reaching the tissue is known to vary with electrode spacing as some current is shunted between the electrodes (Rattay, 1989). We quantified these observations by computing the correlation coefficient between arrays containing peak to peak SSEP amplitudes from all active µECoG channels elicited by stimulation on each electrode pair (Fig. 6). Examination of the confusion matrices resulting from this correlation analysis reveals that while most electrode pairs produce a similar pattern of activity in the somatosensory

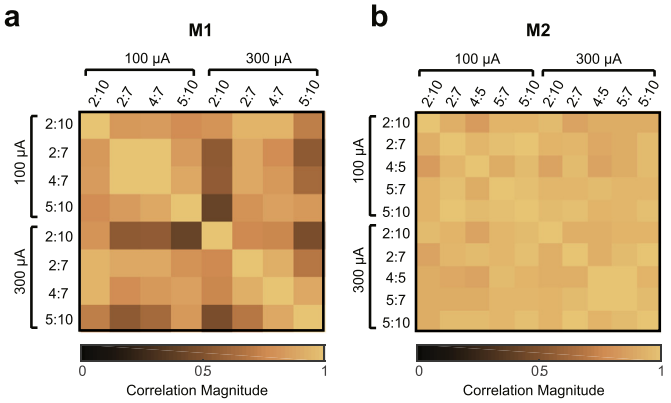

Fig. 6. Confusion matrix describing the correlation between patterns of SSEPs evoked by stimulation on different channels for different current amplitudes. Darker colors denote pairs of channels that evoke different cortical responses. In describing the electrodes used to stimulate the nerve the cathode is always listed first (i.e. 2:10; 2 is the cathode and 10 is the anode). a) Correlation structure in mouse M1 demonstrates differential modulation of cortical activity. b) Stimulation of any electrode pair in mouse M2 tends to evoke similar patterns of cortical activity. (For interpretation of the references to color in this figure legend, the reader is referred to the Web version of this article.)

cortex (i.e. high values of the correlation coefficient), M1 has notable areas where the correlation coefficient between cortical responses is within the 95% CI about zero correlation. Most notably the cortical patterns evoked via stimulation on pairs 2:10 and 5:10 in M1 (Fig. 6a) show little similarity consistent with movement seen in the focus of cortical activation (c.f. Fig. 5a–b).

4. Conclusion

In summary, we have demonstrated the viability of the TF cuff electrode to selectively stimulate the infraorbital branch of the trigeminal nerve of the mouse. The use of thin film fabrication techniques enabled the creation of a flexible, low profile device well suited to the anatomy of the mouse trigeminal nerve that we expect will have negligible impact on the function of the whisker system. The measured electrochemical properties of our TF cuff electrodes were consistent with historical literature for similar materials. The capacitive charge carrying mechanism, based on the impedance and voltage excursion studies, shows that the interface can safely deliver stimulation currents with charge densities up to 73.13 $\mu C/cm^2$ well within the documented limits for safely activating biological tissue (McCreery et al., 1990; Shannon, 1992). Furthermore, the multi-electrode design of the TF cuff permits the selection of different stimulation electrodes to optimize activation of the nerve target. We demonstrated that both the magnitude (Fig. 4) and spatial pattern of cortical activity (Figs. 5 and 6) are modulated by the pair of electrodes selected for stimulation. Future work will examine the longevity and performance of this device as both a stimulation and recording interface for chronic studies examining the therapeutic mechanisms of TNS in the mouse model.

Declaration of interests

The authors declare no competing interests.

Credit author statement

JCW, ZM and AJS conceived the research project. JB, HK, JN and AJS designed the electrode. JB, HK and JN fabricated the electrodes. WZ, JP, WBL and AJS performed the surgeries. JB, HK, JPN, JP and AJS collected the data. JB, JPN and AJS analyzed the data and created figures. JB, JPN, WBL, KAL, JCW, ZM and AJS wrote the paper.

Acknowledgements

The authors would like to thank Sarah Brodnick and Lisa Krugner-Higby for helpful discussions on the surgical approach. This work was funded by the Defense Advanced Research Projects Agency Biological Technologies Office (BTO) Targeted Neuroplasticity Training Program under the auspices of Doug Weber and Tristan McClure-Begley through the Space and Naval Warfare Systems Command Systems Center with (SSC) Pacific grants no. N66001-17-2-4010.

References

Akin, T., Najafi, K., Smoke, R.H., Bradley, R.M., 1994. IEEE Trans. Biomed. Eng. 41, 305–313.
Beekwilder, J.P., Beems, T., 2010. J. Clin. Neurophysiol. 27, 130–138.
Boretius, T., Badia, J., Pascual-Font, A., Schuettler, M., Navarro, X., Yoshida, K., Stieglitz, T., 2010. Biosens. Bioelectron. 26, 62–69.
Box, G.E., Jenkins, G.M., Reinsel, G.C., Ljung, G.M., 2015. Time Series Analysis: Forecasting and Control, fifth ed. John Wiley & Sons, New Jersey.
Brummer, S.B., Turner, M.J., 1977. IEEE Trans. Biomed. Eng. BME-24, 59–63.
Caravaca, A.S., Tsaava, T., Goldman, L., Silverman, H., Riggott, G., Chavan, S.S., Bouton, C., Tracey, K.J., Desimone, R., Boyden, E.S., Sohal, H.S., Olofsson, P.S., 2017. J. Neural Eng. 14, 066005.
Childs, J.E., Alvarez-Dieppa, A.C., McIntyre, C.K., Kroener, S., 2015. J. Vis. Exp., e53032.
Chiluwal, A., Narayan, R.K., Chaung, W., Mehan, N., Wang, P., Bouton, C.E., Golanov, E.V., Li, C., 2017. Sci. Rep. 7, 6792.
Cogan, S.F., 2008. Annu. Rev. Biomed. Eng. 10, 275–309.
Cogan, S.F., Ludwig, K.A., Welle, C.G., Takmakov, P., 2016. J. Neural Eng. 13, 021001.
Cook, I.A., Schrader, L.M., DeGiorgio, C.M., Miller, P.R., Maremont, E.R., Leuchter, A.F., 2013. Epilepsy Behav. 28, 221–226.
DeGiorgio, C.M., Fanselow, E.E., Schrader, L.M., Cook, I.A., 2011. Neurosurg. Clin. 22, 449–456.
DeGiorgio, C.M., Murray, D., Markovic, D., Whitehurst, T., 2009. Neurology 72, 936–938.
Dingle, A., Zeng, W., Ness, J.P., Albano, N., Minor, R.L., Feldman, C., Austin, M., Brodnick, S.K., Shulzhenko, N., Sanchez, R., Lake, W.B., Williams, J.C., Poore, S.O., Suminski, A.J., 2019. J. Neurosci. Methods 324, 108321.
Fanselow, E.E., Nicolelis, M.A.L., 1999. J. Neurosci. 19, 7603–7616.
Fanselow, E.E., Reid, A.P., Nicolelis, M.A.L., 2000. J. Neurosci. 20, 8160–8168.
Farrand, A.Q., Helke, K.L., Gregory, R.A., Gooz, M., Hinson, V.K., Boger, H.A., 2017. Brain Stimul. 10, 1045–1054.
Fisher, R.S., 2011. Epilepsy Behav. 22, 615–616.
Ganzer, P.D., Darrow, M.J., Meyers, E.C., Solorzano, B.R., Ruiz, A.D., Robertson, N.M., Adcock, K.S., James, J.T., Jeong, H.S., Becker, A.M., Goldberg, M.P., Pruitt, D.T., Hays, S.A., Kilgard, M.P., Rennaker, R.L., 2018. eLife 7, e32058.
Henry, T.R., Bakay, R.A.E., Votaw, J.R., Pennell, P.B., Epstein, C.M., Faber, T.L., Grafton, S.T., Hoffman, J.M., 1998. Epilepsia 39, 983–990.
Hitz, C., Lasia, A., 2001. J. Electroanal. Chem. 500, 213–222.
Hudak, E.M., Mortimer, J.T., Martin, H.B., 2010. J. Neural Eng. 7, 026005.
Kuffler, S.W., Nicholls, J.G., 1976. From Neuron to Brain: a Cellular Approach to the Function of the Nervous System, first ed. Sinauer Associates, Massachusetts.
Kumsa, D.W., Bhadra, N., Hudak, E.M., Kelley, S.C., Untereker, D.F., Mortimer, J.T., 2016. J. Neural Eng. 13, 052001.
Lissandrello, C.A., Gillis, W.F., Shen, J., Pearre, B.W., Vitale, F., Pasquali, M., Holinski, B.J., Chew, D.J., White, A.E., Gardner, T.J., 2017. J. Neural Eng. 14, 036006.
Ludwig, K.A., Langhals, N.B., Joseph, M.D., Richardson-Burns, S.M., Hendricks, J.L., Kipke, D.R., 2011. J. Neural Eng. 8, 014001.
Ludwig, K.A., Uram, J.D., Yang, J., Martin, D.C., Kipke, D.R., 2006. J. Neural Eng. 3, 59–70.
Ma, F., Zhang, L., Lyons, D., Westlund, K.N., 2012. Mol. Brain 5, 44.
McCreery, D.B., Agnew, W.F., Yuen, T.G., Bullara, L., 1990. IEEE Trans. Biomed. Eng. 37, 996–1001.
Merrill, D.R., Bikson, M., Jefferys, J.G.R., 2005. J. Neurosci. Methods 141, 171–198.
Micera, S., Navarro, X., 2009. Int. Rev. Neurobiol. 86, 23–38.
Milby, A.H., Halpern, C.H., Baltuch, G.H., 2008. Neurotherapeutics 5, 75–85.
Penry, J.K., Dean, J.C., 1990. Epilepsia 31, S40–S43.
Petersen, C.C.H., 2007. Neuron 56, 339–355.
Plachta, D.T.T., Gierthmuehlen, M., Cota, O., Espinosa, N., Boeser, F., Herrera, T.C., Stieglitz, T., Zentner, J., 2014. J. Neural Eng. 11, 036011.
Pop, J., Murray, D., Markovic, D., DeGiorgio, C.M., 2011. Epilepsy Behav. 22, 574–576.
Rattay, F., 1989. IEEE Trans. Biomed. Eng. 36, 676–682.
Richner, T.J., Thongpang, S., Brodnick, S.K., Schendel, A.A., Falk, R.W., Krugner-Higby, L.A., Pashaie, R., Williams, J.C., 2014. J. Neural Eng. 11, 016010.
Shannon, R.V., 1992. IEEE Trans. Biomed. Eng. 39, 424–426.
Trevathan, J.K., Baumgart, I.W., Nicolai, E.N., Gosink, B.A., Asp, A.J., Settell, M.L., Polaconda, S.R., Malerick, K.D., Brodnick, S.K., Zeng, W., Knudsen, B.E., McConico, A.L., Sanger, Z., Lee, J.H., Aho, J.M., Suminski, A.J., Ross, E.K., Lujan, J.L., Weber, D.J., Williams, J.C., Franke, M., Ludwig, K.A., Shoffstall, A.J., 2019. In: bioRxiv Preprint, Available from: https://doi.org/10.1101/584995.Cited20June2019.
Tyler, D.J., Durand, D.M., 1997. IEEE Trans. Rehabil. Eng. 5, 51–61.
Tyler, D.J., Durand, D.M., 2002. IEEE Trans. Neural Syst. Rehabil. Eng. 10, 294–303.
Veraart, C., Grill, W.M., Mortimer, J.T., 1993. IEEE Trans. Biomed. Eng. 40, 640–653.
Walton, C., Gergely, S., Economides, A.P., 1987. Pacing Clin. Electrophysiol. 10, 87–99.
Wei, X.F., Grill, W.M., 2009. J. Neural Eng. 6, 046008.
Wilks, S.J., Hara, S.A., Ross, E.K., Nicolai, E.N., Pignato, P.A., Cates, A.W., Ludwig, K.A., 2017. Front. Neurosci. 11, 438.
Williams, J.C., Hippensteel, J.A., Dilgen, J., Shain, W., Kipke, D.R., 2007. J. Neural Eng. 4, 410–423.
Yoshida, K., Stein, R.B., 1999. IEEE Trans. Biomed. Eng. 46, 226–234.
Young, R.F., 1995. J. Neurosurg. 83, 72–78.